



A two species thermodynamic Preisach model for the torsional response of shape memory alloy wires and springs under superelastic conditions

Ashwin Rao, A.R. Srinivasa*

Department of Mechanical Engineering, Texas A&M University, College Station, TX 77843-3123, United States

ARTICLE INFO

Article history:

Received 30 July 2012

Received in revised form 23 October 2012

Available online 28 November 2012

Keywords:

Shape memory alloy (SMA)

SMA springs

Superelastic effect

Preisach model

Torsion

Design

ABSTRACT

In this work, a model to simulate the superelastic response for shape memory alloy wires and springs subjected to torsional loading is constructed by combining thermodynamics principles along with Preisach models. Following Doraiswamy et al. (2011), a Gibbs potential based formulation is employed to separate the thermoelastic response of the shape memory alloys from its dissipative response. The dissipative part is then modeled with a discrete Preisach approach. Rather than beginning with a full three dimensional model and solving for non-homogeneous shear stresses across the specimen cross-section, a “strength of materials” approach that can directly model the torsional response using experimentally measurable quantities such as torque and angle of twist is developed. The model results are verified with experiments performed on shape memory alloy springs at three different temperatures. The model is also used to predict torsion response of shape memory alloy wires at different twists and temperatures using experimental results for only one twist or temperature case respectively. The torsional response for three different wire diameters were predicted using experimental data for one diameter case.

© 2012 Published by Elsevier Ltd.

1. Introduction

Shape memory alloys (SMAs) are a subset of a broad class of advanced materials with very interesting properties, viz., shape memory effect (SME) and superelasticity (SE). Their capability to return to a predetermined shape on heating is referred to as the shape memory effect. Their ability to recover large strains (~8%) and associated large stress–strain hysteresis due to mechanical loading–unloading under isothermal conditions is referred to as superelastic/pseudoelastic effect. These reversible effects are manifestations of solid–solid phase transformations between a stable high temperature austenitic phase and low temperature martensitic phase (Khandelwal and Buravalla, 2011). These unique characteristics and the combined sensing and actuation capability of such materials can potentially replace complex multi-component, multi material systems to achieve the desired functionality in many applications like automotive, aerospace, vibration damping and biomedical areas (Ghosh et al., 2013; Wayman, 1992).

In many of these applications, SMAs are typically used in the form of wires, springs, strips, sheets, tubings or bars (nitinolNDC, xxxx; Miyazaki and Otsuka, 1989; Lagoudas, 2008). In particular, SMA springs are most commonly used due to their ability to recover large working strokes (SME) in addition to delivering

near-zero force/stress changes over a large strain increments (SE) (Manhartsberger and Seidenbusch, 1996; Miura et al., 1988). In orthodontic applications, the ability of SMA springs to deliver constant forces is commonly employed for space closure and tooth movement (Miura et al., 1988; Spinella et al., 2010). Stainless steel counterparts can deliver higher forces, however their force delivery rapidly decays over time as compared to SMA springs for relatively long activation ranges (Von Fraunhofer et al., 1993; Schneevogt et al., 1999). In many civil engineering applications, large SMA springs and tubes are being used as damping elements in bridges, buildings and also in seismic resisting systems due to their excellent energy dissipation and recentering capabilities (Speicher et al., 2009). SMA springs and wires are also finding applications as thermal actuators in many pre-commercialized concepts in automotive industry like adjustable mirrors, suspension adjustments for ride comfort, climate control, fuel management etc. (see Fig. 2 from Stoeckel (1990), Bellini et al. (2009) and Spinella et al. (2009) for examples).

In many of these applications, SMA components undergo repeated torsional loading and unloading cycles and hence capturing their full cyclic response is critical. Experimental evidences also suggest that the superelastic response is sensitive to temperature fluctuations which results in force/stress variations (Tripolt et al., 1999; Maganzini et al., 2010). It is thus imperative to model the superelastic response at different operating temperatures to facilitate designers using SMA components under superelastic conditions for different applications.

* Corresponding author. Tel.: +1 979 862 3999; fax: +1 979 845 3081.

E-mail address: asrinivasa@tamu.edu (A.R. Srinivasa).

In one of the first efforts towards modeling hysteretic response of SMA members under torsion, [Tobushi and Tanaka \(1991\)](#) used Tanaka's constitutive model ([Tanaka, 1986](#)) to analyse axially loaded helical springs by assuming each segment is under pure torsion. They treated the springs to be perfectly plastic and derived the constitutive relations by neglecting hardening/softening responses during phase transformation. These assumptions greatly simplify the solution, however experimental evidence show that the hardening response cannot be neglected in SMA responses for polycrystalline SMA ([Mirzaeifar et al., 2010a](#)). It is also difficult to incorporate temperature effects in the superelastic response by using such an approach.

[Mirzaeifar et al. \(2010b\)](#) in their work considered analysis of circular SMA bars subjected to pure torsion. They reduce three dimensional constitutive equations developed by [Boyd and Lagoudas \(1996\)](#) and [Qidwai and Lagoudas \(2000\)](#) for the case of pure torsion and thus derive explicit relationship for shear stress. They divide the wire cross section into three zones – an inner austenitic core, a transition region and an outer martensitic layer (see [Fig. 1](#)) to derive relations for each of the divided regions under different twist angles by integrating state variables across the three zones (Expression 25 from [Mirzaeifar et al. \(2010b\)](#)). They further extend this idea in their sequel work to study SMA helical springs by considering the spring both as straight SMA bars and curved SMA bars (to include curvature effects) subjected to torsional loading ([Mirzaeifar et al., 2010a](#)). [Chapman et al.](#) also reduce the 3D model developed by [Boyd and Lagoudas \(1996\)](#) and [Qidwai and Lagoudas \(2000\)](#) to predict torsional response with an implementation in Abaqus for a FE simulation ([Chapman et al., 2011](#)). Such strategies are extremely cumbersome for identification of material and model parameters from experimental data and incorporating temperature changes ([Table 1](#) in [Mirzaeifar et al. \(2010a\)](#), [Mirzaeifar et al. \(2010b\)](#) and [Chapman et al. \(2011\)](#) lists the number of material parameters needed for model verification). Furthermore, a close perusal of the 3-D constitutive models developed, reveals that, in actuality, these approaches just use the one dimensional data and use a von-Mises equivalent stress approach due to lack of a full three dimensional data on SMAs. Given the fact that such an approach (originally based on experimental observations of steel) does not even work well for aluminum, it is hard to justify their use in SMA given their complex thermomechanical response.

[Aguir et al. \(2010\)](#) in their work simplify the 1-D constitutive model developed by [Paiva et al. \(2005\)](#) and [Savi and Paiva \(2005\)](#)

Table 1

Values of thermodynamical parameters employed for model verification in case of springs.

Parameters	Corresponding values
G_a	14.4 GPa
G_m	10.56 GPa
B	−9.6 N mm
a	151.34 Nmm
b	−0.38 N mm/K
θ_1	348 K
θ_2	373 K
θ_3	398 K

by replacing the corresponding terms for normal stress, strains and elastic modulus by its counterparts shear stress, shear strains and shear modulus respectively. The authors discuss three different representations for shear stress and martensitic volume fraction distributions and use “homogeneous phase transformation” represented by [Fig. 2\(c\)](#) in [Aguir et al. \(2010\)](#).

The von-Mises equivalent stress approach or the assumption that phase transformations are homogeneous across the wire are not completely realistic as the phase transformation front gradually moves from the outer fibers towards the neutral axis as the wire twists under torsion and its location is not known a priori ([Tobushi and Tanaka, 1991](#); [Mirzaeifar et al., 2010a](#); [Mirzaeifar et al., 2010b](#)). They can be possibly determined only if the prior deformation history is known. Further, the shear strain tends to zero at the core of the specimen cross-section as the wire twists ([Aguir et al., 2010](#)). This implies that the possibility of having a fully transformed case can only be possible if the angle of twist asymptotically reaches infinity ([Doaré et al., 2011](#)). A schematic in [Fig. 1](#) shows the three zones – an inner austenitic core, a transition region and an outer martensitic layer. The untransformed austenitic core at the center might exist even for the maximum possible twist due to really small shear strains. [Fig. 1](#) also depicts the non-linear shear stress variation across the wire cross-section. All of these suggest that the transition across the wire cross-section is not homogeneous and cannot be accounted for easily by just averaging or integrating certain state variables in constitutive relations across the wire cross sections.

To overcome these issues, a “strength of materials approach for smart materials” is proposed by constructing a simple model based on experimentally measurable quantities torque and angle of twist, rather than solving for non-homogeneous shear stresses and strains across the wire cross-section and then integrating. It is clear that the model is limited to torsional deformations alone and hence is not a general approach. However, as the theories of beams and rods have shown, these approaches are extremely useful for designers as they can faithfully simulate the response with a minimum computations when compared to a full 3-D approach. The main advance from a purely mechanical theory of torsion is the incorporation of thermal response by means of a thermodynamical approach combined with a Preisach model in simulating response of superelastic SMA wires and springs ([Mayergoyz, 1986](#); [Mayergoyz and Service, 2003](#); [Doraiswamy et al., 2011](#)). The key idea here would be in separating the elastic and the dissipative part of the hysteretic response with a Gibbs potential based formulation. [Doraiswamy et al. \(2011\)](#) in an earlier work have shown the advantages of using such an approach in simulating superelastic responses with multiple internal loops and an improved treatment of temperature dependence associated with superelastic responses of SMA wires (refer [Figs. 9 and 10](#) in [Doraiswamy et al. \(2011\)](#)). With the inclusion of both thermal and mechanical loading in the same framework, there is a greater connection with the thermodynamics of the response and an added capability of simulating

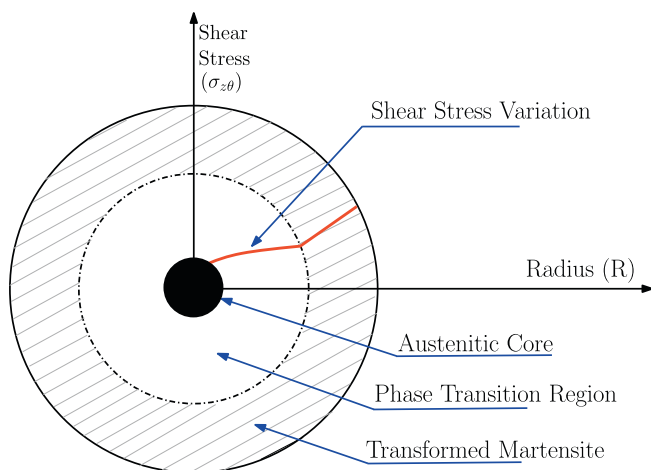


Fig. 1. Non linear shear distribution across the wire cross-section under torsional loading with an inner austenitic core, a phase transition region and an outer transformed martensitic layer ([Mirzaeifar et al., 2010b](#)).

both load and displacement controlled experiments. With such an approach, it is not necessary to use different approaches for stress and temperature driven phase changes as observed with SMA response. In addition, a model that is capable of predicting torque v/s angle of twist response directly could facilitate designers greatly especially in designing springs under superelastic conditions for biomedical and civil engineering applications.

2. Organization of this paper

The remaining sections of the paper are organized as follows: In Section 3, experiments performed on NiTi SMA Springs at Texas A&M University are presented. Next in Section 4, a Gibbs potential based model is developed to simulate superelastic response of SMA springs in order to obtain thermodynamic driving force and the volume fraction of martensite, by separating the thermoelastic and the dissipative part of the hysteretic response. Further in Section 5, a Preisach Model used to handle the dissipative part of the superelastic SMA response is discussed. In Section 6, parameter identification for a given superelastic response is detailed. In Section 7, some salient features of the model along with the simulation procedure are briefly discussed. Next in Section 8, the model predictions are compared against experimental results on SMA springs and on SMA wires obtained from Chapman et al., (2011) and Doaré et al. (2011). Finally in Section 9, the highlights of this work are summarized.

3. Material and experimental set-up

NiTi springs (martensitic at room temperature) with a composition details in element weight % (Ni-55.91, Balance Ti, trace elements <0.25) were obtained from Images SI Inc. The listed transformation temperature (A_f) as reported by the supplier is in the range of 318–328 K. The spring specifications are as follows.

- Mean coil diameter of the spring “ D_m ” = 6 mm
- Wire diameter “ d ” = 0.75 mm
- Spring Index “ C_m ” = 8
- Number of active coils “ n ” = 20.

An Instron 5567 series uniaxial tensile testing machine was used to carry out cyclic loading–unloading experiments at various temperatures on the spring samples. An Instron SFL Heatwave environmental chamber (Model: 3119–506 Heatwave 240) was employed for maintaining precise air temperature throughout the length of the experiment. A 2716 series mechanical wedge-action grips with additional hooks were used to hold the extension springs inside the temperature chamber. Fig. 2 shows the experimental set-up used along with the grip and specimen mounting details. All the tests were conducted after the environmental chamber equilibrated at the desired temperature. The chamber employs two Inconel sheathed 3 mm diameter type K thermocouples with online temperature display on the chamber control panel. In addition to this, external “K” type thermocouples were used to monitor the specimen temperature directly.

3.1. Test methodology

Constant temperature displacement controlled uniaxial tests were conducted on the extension springs that were subjected to a axial displacement of 75 mm and then unloaded. A constant displacement rate of 15 mm/min was employed throughout the length of the experiment. Force (P) and spring extension (δ) data were monitored and recorded as a function of time using Instron's

customized Bluehill 2.0 software with the help of in built 5 kN capacity load cell and the crosshead displacement respectively.

The torque applied on any cross section of the spring wire can be computed using the expression

$$T = P \left(\frac{D_m}{2} \right) \quad (1)$$

Assuming that the angle of twist is uniform over the entire length of the active coils and ignoring curvature effects, the angle of twist per unit length (ϕ) can be evaluated in terms of the spring displacement as

$$\phi = \frac{2\delta}{\pi D_m^2 n} \quad (2)$$

It is observed that these two results (Eqs. (1) and (2)) are independent of each other with the former being purely kinetic and the latter being purely geometrical in nature. No constitutive theory relating the torque to the angle of twist is necessary for these results to be established.

The tests were performed at room temperature (298 K) to simulate shape memory effect and three other temperatures above A_f viz. 348, 373 and 398 K to observe superelastic behavior of SMA springs. Four trials were conducted under each test condition to ensure repeatability of results.

3.2. Experiments: results and discussion

The Force – extension results of the SMA spring as obtained from the Instron machine for different temperatures are illustrated in Fig. 3(a). The corresponding Torque-angle of twist results using Eqs. (1) and (2) are shown in 3(b). As seen in Fig. 3(a), for 298 K trial, there is a residual elongation of about 50 mm observed upon unloading which can be recovered completely upon heating to a temperature above A_f . In the trials pertaining to higher temperatures 348, 373 and 398 K, the spring is austenitic at the start of the test and demonstrates near perfect pseudoelasticity with the complete recovery of applied deformation. In each of these cases, the springs are partially transformed to stress induced martensite (SIM) and the extent of transformation from austenite to SIM is different in each temperature trial. This is due to the fact that the higher the temperature above A_f , the higher is the critical stress required for transformation and thus lesser is the transformation from austenite to SIM when compared against the same maximum deformation (75 mm) of the spring. It can also be observed from Fig. 3(a) that the stiffness increases and the hysteresis area decreases with the increase in the working temperature above A_f .

4. Model development

Consider a wire subjected to a torque “ T ” about its axis or a helical extension SMA spring subjected to force “ P ” along its spring axis and let the corresponding axial displacement be denoted by “ δ ”. Let,

- “ D_m ” be the mean coil diameter of the spring in mm
- “ d ” be the SMA wire diameter in mm.
- “ C_m ” denote the Spring Index.
- “ n ” be the number of active coils (i.e neglecting the end hooks).

The torque (T) and angle of twist per unit length (ϕ) are directly measured in the case of wire and the same can be computed using Eqs. (1) and (2) for springs respectively.

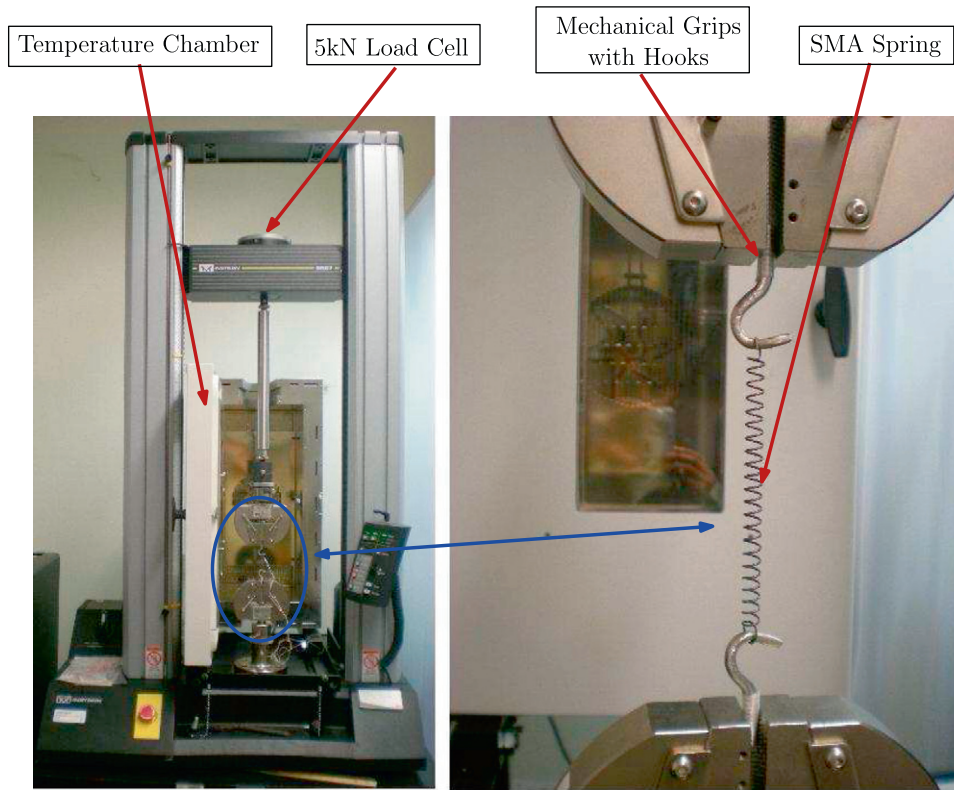


Fig. 2. Experimental set-up showing Instron uniaxial tensile testing machine with a temperature chamber and mounting of a SMA extension Spring between mechanical wedge grips and hooks.

4.1. The Gibbs potential

The superelastic response of SMA wire or springs is formulated by assuming a form for Gibbs potential per unit volume (inspired from Doraiswamy et al. (2011) and Rajagopal and Srinivasa (1999)) that is a function of the torque (T), working temperature (θ) and the extent of transformation (α) in the cross section i.e the volume fraction of martensite formed during phase transition (see Fig. 1).

The Gibbs potential (\mathcal{G}) is assumed to be composed of (refer Eq. (3)):

1. a linear combination of the torsional strain energy of the two phases,
2. an interaction term between the two phases,
3. a term related to the heat capacity difference between the two phases and
4. a term relating to the heat capacity of the austenite.

Specifically the Gibbs potential energy per unit reference volume is assumed to be of the form,

$$\mathcal{G} = - \left(\underbrace{\frac{\alpha T^2}{2G_m J} + \frac{(1-\alpha)T^2}{2G_a J}}_1 + \underbrace{B\alpha(\alpha-1)}_2 + \underbrace{(1-\alpha)(a+b\theta)}_3 - \underbrace{C\theta(1-\ln\theta)}_4 \right) \quad (3)$$

where, α is the martensite volume fraction, T is the applied torque, G_a and G_m are the austenitic and martensitic shear moduli, $J = \frac{\pi d^4}{32}$ is the Polar Moment of Inertia, B , a and b are constants, θ is the operating temperature and C is the specific heat. The constant “ B ” represents the interaction energy between the austenite and martensite phases while “ b ” is the entropy difference between the

austenite and martensite phases respectively (see Eq. (5) below). Constant “ a ” is the internal energy difference between the austenite and martensite phases at 0 K (see Eq. (7) below). The method to identify the above parameters will be described later in Section 6.

4.2. Establishing driving force

From classical thermodynamics, the entropy is given by,

$$\eta = - \frac{\partial \mathcal{G}}{\partial \theta} = -C \ln \theta - (1-\alpha)b \quad (4)$$

Using above,

$$\left. \begin{aligned} \eta|_{(\alpha=1)} &= -C \ln \theta \\ \eta|_{(\alpha=0)} &= -C \ln \theta - b \end{aligned} \right\} \Rightarrow b = \Delta \eta = \eta|_{(\alpha=1)} - \eta|_{(\alpha=0)} \quad (5)$$

thus, b is the entropy difference between the austenite and martensite states.

The internal energy, Ξ , is given by,

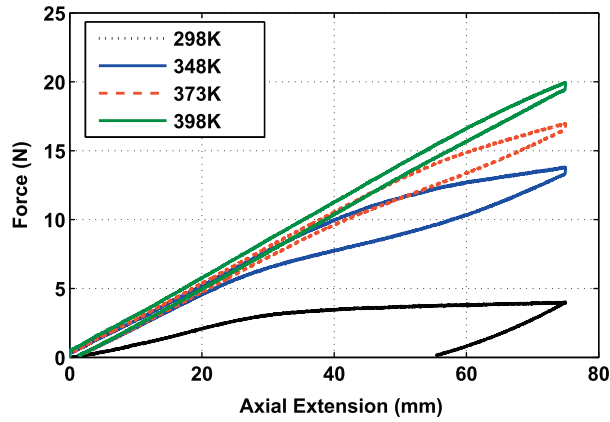
$$\begin{aligned} \Xi &= \mathcal{G} - \theta \frac{\partial \mathcal{G}}{\partial \theta} \\ &= - \left(\frac{\alpha T^2}{2G_m J} + \frac{(1-\alpha)T^2}{2G_a J} \right) + B\alpha(\alpha-1) + (1-\alpha)a - C\theta \end{aligned} \quad (6)$$

Using above,

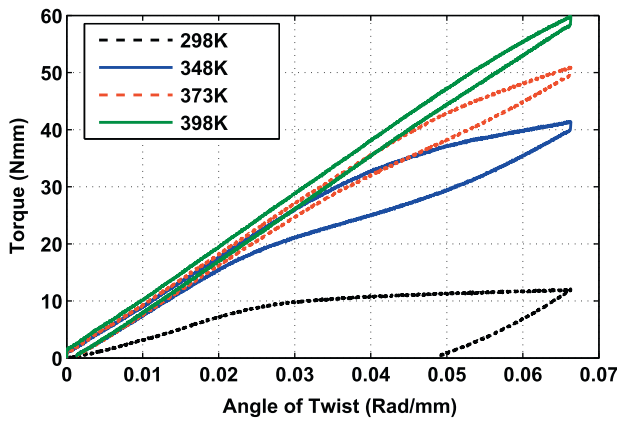
$$\left. \begin{aligned} \Xi_A &= \Xi|_{(\alpha=0, T=0, \theta=0)} = a \\ \Xi_M &= \Xi|_{(\alpha=1, T=0, \theta=0)} = 0 \end{aligned} \right\} \Rightarrow a = \Xi_A - \Xi_M \quad (7)$$

From the above, the parameter a is the internal energy difference between the two phases at 0 K.

From the Gibbs potential, the elastic part of the angle of twist is given by,



(a) Isothermal Force v/s axial extension results as measured using the Instron setup shown in figure 2



(b) Force v/s Axial extension of spring converted to Torque v/s angle of twist using equations 1 and 2

Fig. 3. Results of tests conducted on NiTi SMA Springs at temperatures 298, 348, 373 and 398 K with 15 mm/min displacement rate for all cases. The results for 348, 373 and 398 K show superelastic response of SMA springs. The extent of transformation in each high temperature trial is different when compared against the same maximum spring elongation (75 mm) or corresponding twist. Eqs. (1) and (2).

$$\phi_e = -\frac{\partial \mathcal{G}}{\partial T} = \frac{\alpha T}{G_m J} + \frac{(1-\alpha)T}{G_a J} \quad (8)$$

Also, the Helmholtz potential ψ , is related to Gibbs potential \mathcal{G} , by,

$$\psi = \mathcal{G} - T \frac{\partial \mathcal{G}}{\partial T} \quad (9)$$

The difference between the rate of external working ($T\dot{\phi}$) and the rate of change of the Helmholtz potential keeping the temperature fixed ($\dot{\psi}|_{\theta}$), must be equal to the macroscopic inelastic power (P_{inel}). In other words,

$$P_{inel} = T\dot{\phi} - \dot{\psi}|_{\theta} \quad (10)$$

Using Eqs. (8), (9) and upon further simplification,

$$T(\dot{\phi} - \dot{\phi}_e) - \frac{\partial \mathcal{G}}{\partial \alpha} \dot{\alpha} = P_{inel} \quad (11)$$

From Eq. (11), it is observed that there are two contributions to the inelastic power, one from the shape change that occurs due to phase transition ($T(\dot{\phi} - \dot{\phi}_e)$) and the other from the Gibbs potential difference between the two phases ($-\frac{\partial \mathcal{G}}{\partial \alpha} \dot{\alpha}$). The recoverable angle of twist is due to the phase transformation and is proportional to the extent of transformation depending on the axial force and

corresponding axial displacement that the spring is subjected to. The maximum angle of twist ϕ_{max} corresponding to a maximum transformational strain that can assumed to be of the order of 6%.

$$\dot{\phi} - \dot{\phi}_e = \phi_{max} \dot{\alpha} \Rightarrow \phi - \phi_e = \phi_{max} \alpha \quad (12)$$

In the above equation note that, when $\alpha = 1$, $\phi - \phi_e = \phi_{max}$ and when $\alpha = 0$, $\phi - \phi_e = 0$. Now substituting Eqs. (12) into (11), it is now possible to identify the driving force for the phase transformation in the superelastic response of the SMA springs or wires as shown below

$$\left(T\phi_{max} - \frac{\partial \mathcal{G}}{\partial \alpha} \right) \dot{\alpha} = P_{inel} \quad (13)$$

$$\mathcal{F} = T\phi_{max} - \frac{\partial \mathcal{G}}{\partial \alpha} \Rightarrow \mathcal{F} \dot{\alpha} = P_{inel} \quad (14)$$

Note that the net driving force is the difference between the applied torque and the chemical potential for phase change, so that, in the absence of hysteresis, phase change would occur if this driving force is positive. The rate of mechanical dissipation, ξ , is the net macroscopic inelastic work (P_{inel}) in a closed cycle of state and this is non-negative by the second law of thermodynamics (Ghosh and Srinivasa, 2011), i.e.,

$$\xi = \oint P_{inel} dt \geq 0 \quad (15)$$

4.3. Driving force & volume fraction estimation using experimental data

The driving force and volume fraction expressions can be evaluated using Eqs. (3) and (13) and is given by Eq. (16) below.

$$\mathcal{F} = T\phi_{max} + T^2 \left(\frac{1}{2G_m J} - \frac{1}{2G_a J} \right) - B(2\alpha - 1) + b\theta + a \quad (16)$$

It is clear from the above expression that driving force is a function of torque (T), angle of twist (ϕ), martensitic volume fraction (α), and temperature (θ). The variables torque, angle of twist and temperature are nondimensionalized before proceeding further with the derivations. The nondimensionalized variables are: $T^* = T/T_{max}$, $\phi^* = \phi/\phi_{max}$, $\theta^* = \theta/\theta_{max}$. Experimental results for 348 K were chosen as reference for simulation. Henceforth, for better readability, the *'s will be omitted from the nondimensionalized variables. Further, an expression for the martensitic volume fraction evolution (α) can be obtained using expressions (8) and (12). The volume fraction evolution expression α can be obtained from the Torque-angle of twist experimental data and the assumed form of Gibbs potential.

$$\alpha = \frac{\phi - \frac{T}{G_a J}}{\frac{T}{G_m J} - \frac{T}{G_a J} + 1} \quad (17)$$

Using expressions (17) and (16), each experimental data point from Torque vs angle of twist plot can be reduced to corresponding driving-force – volume fraction plot as shown in Figs. 4 and 5 (i.e. (T, ϕ) to (\mathcal{F}, α)). Experimental results for one particular case are chosen as reference for establishing these driving-force – volume fraction plots.

Until this stage, a thermodynamical framework was employed to derive driving-force – volume fraction relationships as typically used in modeling phase transforming materials. Now, following the approach of Doraiswamy et al. (2011), rather than specifying a “plasticity-like” evolution equation for $\dot{\alpha}$ as typically done for SMAs (see Boyd and Lagoudas (1996) and Qidwai and Lagoudas (2000)), a Preisach type model will be used to capture change in α . As noted previously, phase transitions are actually more akin to domain switching in magnetism rather than crystallographic slip and hence a Preisach model is more appropriate here. A Preisach

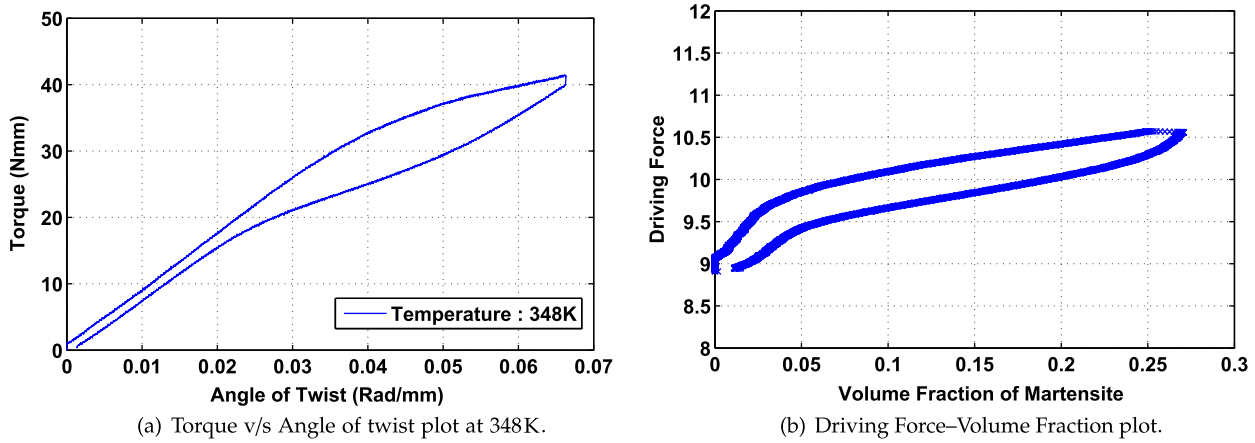


Fig. 4. Experimental torque v/s angle of twist data is reduced to driving force – volume fraction plot using thermodynamic principles by using Eqs. (17) and (16).

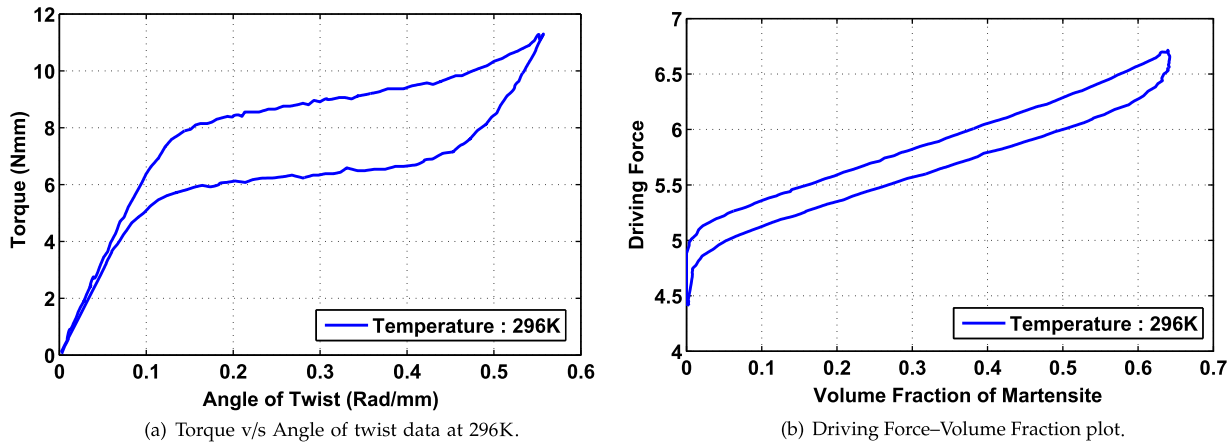


Fig. 5. Experimental torque v/s angle of twist data is reduced to driving force – volume fraction plot using thermodynamic principles by using Eqs. (17) and (16). Experimental data obtained from Chapman et al. (2011).

model would be used for the relationship between driving force \mathcal{F} and volume fraction α . This way one has to now focus purely on the hysteretic dissipative response and not on the entire reversible thermoelastic response. Furthermore, this approach of using Preisach model varies from the conventional Preisach models that are commonly employed to mimic hysteresis where the stress–strain (Ortín, 1992) or temperature–strain relationships (Ktena et al., 2001; Bo and Lagoudas, 1999) are directly modeled with Preisach elements. The present approach also can simulate both load and displacement controlled experiments.

5. Preisach model development

The traditional Preisach models (Mayergoyz, 1986; Mayergoyz and Service, 2003) assembles a series of basic hysteretic elements or hysterons to represent hysteresis. Each hysteron (see Fig. 6) behaves like a non-ideal switch that switches on when the load increases beyond $F_{forward}$, giving an “output”, $\Delta\alpha_i$, and switches off at $F_{backward}$. With the establishment of the driving force and extent of transformation expressions, the thresholds for the hysteron are $F_{forward}$ and $F_{backward}$ and the output being volume fraction. With the use of large number of hysterons in series that turn on and off at different driving force values, contribution of each hysteron to volume fractions can be obtained. The following algorithm (see Appendix A) details the process by which the contribution of each

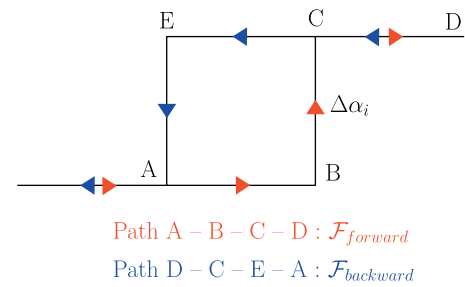


Fig. 6. Basic hysteretic element or hysteron used in the current discrete Preisach Model. Directions of allowed transformations are represented by the arrows on the hysteron. Each hysteron behaves like a non-ideal switch that switches on when the torque increases beyond $F_{forward}$ with an output of $\Delta\alpha_i$ and switches off at $F_{backward}$.

hysteron is accumulated to get the total volume fraction of martensite for a given driving force.

5.1. Algorithm for obtaining Preisach parameters

For purposes of completeness, the algorithm used by Doraiswamy et al. (2011) for obtaining the Preisach parameters is summarized in Appendix A.

5.2. Preisach triangle

Following Doraiswamy et al. (2011), the geometric arrangement of hysterons in a systematic way is with the help of a Preisach Triangle (Chapter 1 Mayergoyz and Service, 2003). The hysterons with the lowest forward driving force ($\mathcal{F}_{forward}$) are positioned at the bottom of the triangle and the highest ones are arranged at the top end. Similarly, for the backward driving force hysterons ($\mathcal{F}_{backward}$), they are arranged such that they increase from left to right i.e. the lowest ones to the left and the highest ones to the right. Further, the hysterons on any particular row have the same $\mathcal{F}_{forward}$ values and similarly the hysterons on any column have the same $\mathcal{F}_{backward}$ values in the triangle (Fig. 13). Once the $\mathcal{F}_{forward}$ and $\mathcal{F}_{backward}$ values are assigned, the corresponding “output”, $\Delta\alpha$ for each hysteron needs to be evaluated. By assigning hysterons at specific positions on a Preisach triangle, the three parameters $\mathcal{F}_{forward}$, $\mathcal{F}_{backward}$ and $\Delta\alpha$ are automatically estimated. The number of hysterons in a triangle of side n is $\frac{n(n+1)}{2}$.

$\Delta\alpha$ for each hysteron can be evaluated by setting up a system of equations where each equation corresponds to the sum of the outputs of all those hysterons that are switched on. By equating these to the volume fraction (α) from the data (i.e. from Figs. 4(b) or 5(b)) corresponding to the driving force level. It is evident that there are $\frac{n(n+1)}{2}$ hysterons and only $k \left(< \frac{n(n+1)}{2} \right)$ data points (depending on the experimental data). This problem is solved using least squares technique with a non-negativity constraint for the outputs of the hysterons. A “lsqnonneg” package from MATLAB® is readily available to compute this.

6. Parameter identification

The model parameters can be separated into sets of parameters arising from thermodynamical framework and those from the Preisach models related to hysterons. Section 5 referred to the details of obtaining Preisach model related parameters described in Fig. 6.

In this section, the identification of parameters G_a , G_m , B , a and b are discussed. These arise from the thermodynamical framework formulated by assuming a form for Gibbs potential (refer Eq. (3)). The values used for these parameters in the model are reported in Table 1 and are determined keeping the experimental data of springs as reference. The parameters for predicting other wire responses can be estimated similarly as detailed below.

- “ G_a ” and “ G_m ” being the austenitic and martensitic shear moduli can be estimated directly from the experimental data by finding the initial slopes of the superelastic response at 348 K and the shape memory response at 298 K respectively. The shear moduli can also be evaluated by assuming the austenitic and martensitic elastic moduli and a Poisson's ratio in the range 0.3–0.4 for both the cases as reported in the literature (refer Table 1 in both Mirzaeifar et al. (2010a,b)).
- “ B ” is the coefficient of the interfacial energy term related to the area of hysteresis (as shown in Rajagopal and Srinivasa (1999)). Therefore parameter “ B ” is proportional to the area of hysteresis under torque-angle of twist plot. A value for “ B ” is chosen in order to obtain a good fit between the model and the experimental hysteresis.
- The computation of entropy difference “ b ” can be justified by the comparing responses at two different temperatures for the same extent of transformation α as shown below. If \mathcal{F}_1 is the driving force at torque T_1 and temperature θ_1 and \mathcal{F}_2 is the corresponding driving force at torque T_2 and θ_2 respectively.

$$\mathcal{F}_1 = \frac{T_1^2}{2} \left(\frac{1}{G_m J} - \frac{1}{G_a J} \right) + a + b\theta_1 - B(2\alpha - 1) + T_1 \phi_{max} \quad (18)$$

$$\mathcal{F}_2 = \frac{T_2^2}{2} \left(\frac{1}{G_m J} - \frac{1}{G_a J} \right) + a + b\theta_2 - B(2\alpha - 1) + T_2 \phi_{max} \quad (19)$$

$$\mathcal{F}_1 - \mathcal{F}_2 = \frac{T_1^2 - T_2^2}{2} \left(\frac{1}{G_m J} - \frac{1}{G_a J} \right) + b(\theta_1 - \theta_2) + (T_1 - T_2) \phi_{max} \quad (20)$$

The driving force analogous to chemical potential (see Callen (1985)) does not change with temperature and therefore $\mathcal{F}_1 - \mathcal{F}_2 = 0$. Using this relation and further neglecting the terms arising due to modulus differences a relation for b is obtained as shown below.

$$b = - \frac{T_1 - T_2}{\theta_1 - \theta_2} \phi_{max} \quad (21)$$

It can be seen that the value of “ b ” (from Table 1) matches with the values available in the literature for SMA (see Bo et al. (1999)).

- The parameter “ a ” serves as a datum for the driving force and is computed by setting the driving force to be zero at the stress-free austenite phase at 373 K, i.e.,

$$\mathcal{F}|_{\alpha=0, T=0} = a + b\theta + B \quad (22)$$

$$a = -b\theta - B \quad (23)$$

7. Torque vs angle of twist response – model prediction

The algorithm described in Appendix A is used to estimate the volume fraction α for a given driving force \mathcal{F} . The protocol of finding the original Torque - Angle of twist under both load and displacement controlled tests is illustrated below.

7.1. Load (Torque) controlled protocol

If at time t_i , $T(i)$, $\phi(i)$ and $\theta(i)$ are assumed to be known then by using Eq. (17), $\alpha(i)$ can be evaluated. In order to compute these variables at time t_{i+1} , it is assumed that $T(i+1)$ is known. $\mathcal{F}(i+1)$ can now be computed from Eq. (16) for a known $\alpha(i)$. Once $\mathcal{F}(i+1)$ is evaluated, the Preisach model is used to predict $\alpha(i+1)$. With $\alpha(i+1)$ and $T(i+1)$ now known, using Eq. (8) to find $\phi_e(i+1)$ and hence $\phi(i+1)$ from Eq. (12).

7.2. Displacement (Angle of Twist) controlled protocol

If at time t_i , $T(i)$, $\phi(i)$ and $\theta(i)$ are known then by using Eq. (17) $\alpha(i)$ can be evaluated. Here $\phi(i+1)$ is known and $T(i+1)$ needs to be computed. $\mathcal{F}(i+1)$ is computed using Eq. (16). Now the Eq. (17) is used to express T in terms of ϕ and α . The Preisach model is used again to find $\alpha(i+1)$ from $\mathcal{F}(i+1)$. Once $\alpha(i+1)$ and $\phi(i+1)$ are evaluated, using Eq. (17), $T(i+1)$ is evaluated.

7.3. Simulation of torque vs angle of twist response at different temperatures for springs and wires

Once the test protocol as highlighted in Sections 7.1 or 7.2 are the model predictions as compared with the experimental results described in Section 3 are described here. For prediction of response of springs considered here, a total of 5050 hysterons which is an equivalent to a Preisach triangle with a side of 100 were employed. In case of wires a total of 20100 hysterons which is an equivalent of a Preisach triangle with a side of 200 were used.

8. Results and discussion

8.1. Simulations of SMA spring and wire response using complete Torque vs Angle of Twist Data

Figs. 7 and 8 shows the model prediction at 348 K and 296 K respectively with the corresponding experimental results used for comparison. The model shows a good fit with the experimental results and can estimate the hysteresis accurately.

8.2. Simulation of SMA wire response at different twists

Doaré et al. (2011) in their work performed quasi-static tests on 2 mm dia SMA wires for three different angle of twists (100° , 350° and 450°). The 450° data was used as reference to calibrate the model with the assumption that it is the maximum possible angle of twist that the sample can encounter without failing. The hysteresis generated by the 450° degrees data are used to predict responses at any other angle of twist without recomputation of any model parameters. Fig. 9(a) and (b) shows the model predictions at different angles of twist 350 and 225 degrees twist respectively using the hysteresis generated with the 450° degrees twist. The model predictions show a close match with the experimental results.

It must be highlighted that the possibility of having a fully transformed case can only be possible if the angle of twist asymptotically reaches infinity due to really small shear strains at the core. This suggests that only a partially transformed case is possible in case of torsional loading. Thus the “maximum angle of twist” for any sample must be assumed for any model predictions using this approach.

8.3. Simulation and model predictions for SMA components at different temperatures

Experimental evidences in many tension tests indicate that the plateau stress in a superelastic response translates linearly with temperature and a linear assumption ($a + b\theta$ terms in the model) is one of the simplest ways to capture the temperature dependence of superelastic responses in SMA (see experimental results – Fig. 7 in Liang and Rogers (1990), Fig. 12 in Müller and Seelecke (2001), Fig. 12 in Otsuka and Ren (2005), Fig. 3 in Shaw and Kyriakides (1995), Fig. 3 in Shaw (2000) etc. for illustrations). This linear assumption is extended for the torsion loading case for prediction

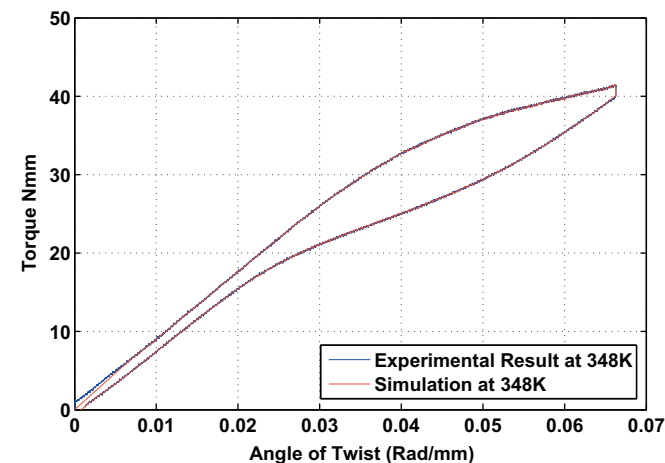


Fig. 7. Model prediction for the superelastic response of SMA spring at 348 K. Model prediction and experimental results show a good match. This is not surprising since the Preisach parameters were chosen to fit the data. However the closeness of the fit is an indication of the power of the Preisach approach.

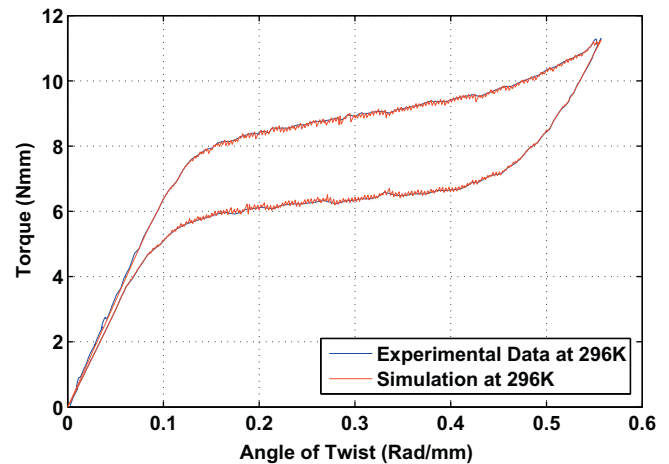
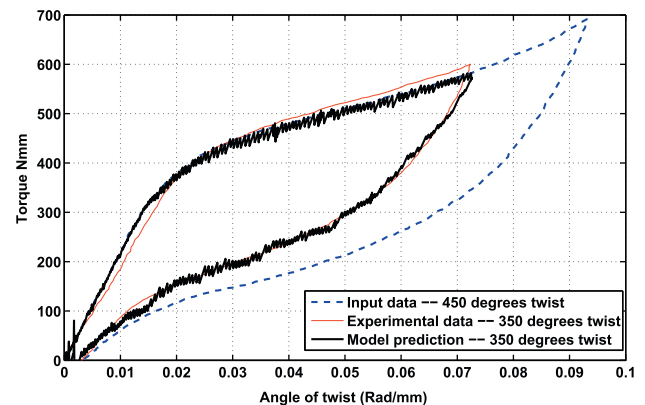
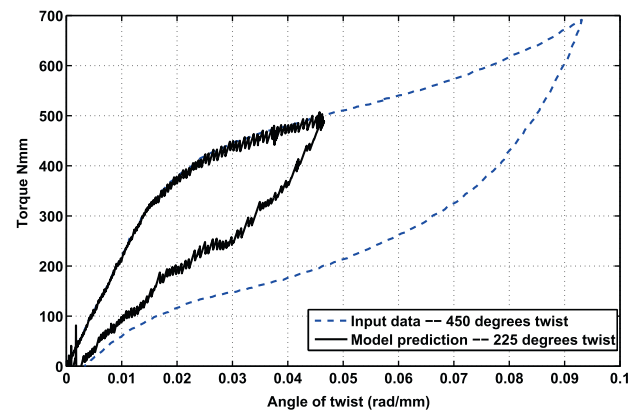


Fig. 8. Model prediction for the superelastic response of SMA wire tested at 296 K showing a good match. Experimental results at 296 K were obtained from Chapman et al., (2011). The jaggedness of the model simulation is due to the fact that a discrete Preisach model was used.



(a) Model prediction for 350 degrees twist using 450 degrees twist as input data. Model results show a close match with the experimental results with an average error $\sim 6.5\%$



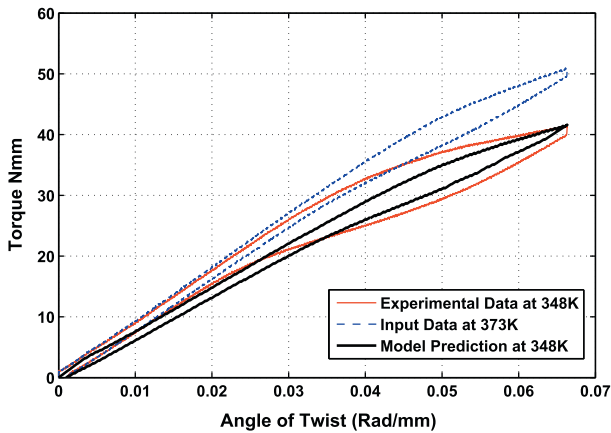
(b) Model prediction for 225 degrees twist using 450 degrees twist as input data

Fig. 9. Prediction for responses at 350 and 225 degrees twist using the hysteresis generated at 450 degrees twist. The experimental results for all cases were obtained from Doaré et al. (2011).

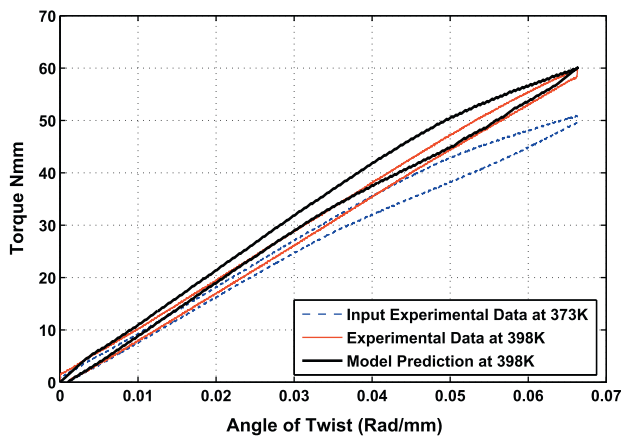
of responses at different temperatures. Hence, it was assumed that the driving force does not change with temperature if compared for the “same extent of transformations (α)”. As shown in Eq. (19), the driving force expressions are estimated for the same martensitic volume fraction α at two different temperatures θ_1 and θ_2 .

8.3.1. Simulation and model predictions for SMA spring response at different temperatures

Fig. 10(a) and (b) shows the model prediction at temperatures 348 and 398 K using the hysterons generated with the 373 K results as the data input. The predictions do not match exactly due to the fact that extent of transformation at 373 K is different when compared to that in case of 348 or 398 K results. The springs undergo only partial transformation from austenite to SIM at different temperatures above A_f . As seen in the experimental results from Fig. 3(a), the higher the temperature above A_f , the lesser is the transformation from austenite to SIM and thus lesser is hysteresis area when compared against the same maximum deformation (75 mm) of the spring. The model predictions for different temperatures could match exactly if the superelastic responses at different temperatures are compared for the “same extent of transformation” for each temperature case. The model predictions at different temperatures would be over or under estimated based on the choice of temperature that is used to generate the hysterons for prediction. It has to be noted that hysteron parameters in this current estimation do not have to be recomputed to predict the response at different temperatures. If one needs to predict the



(a) Model prediction for 348K compared with the corresponding experimental data



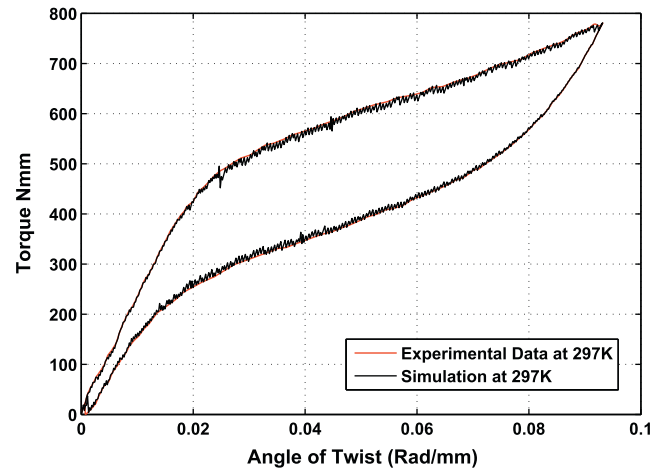
(b) Model prediction for 398K compared with the corresponding experimental data

Fig. 10. Prediction for responses at temperatures 348 and 398 K using the hysterons generated from 373 K. The prediction doesn't match exactly due to the fact that the extent of transformation at 373 K is different when compared to that in case of 348 or 398 K results. (details in Section 8.3.1). The average error for this case was 8.7% and 5.2% for 348 and 398 K predictions respectively.

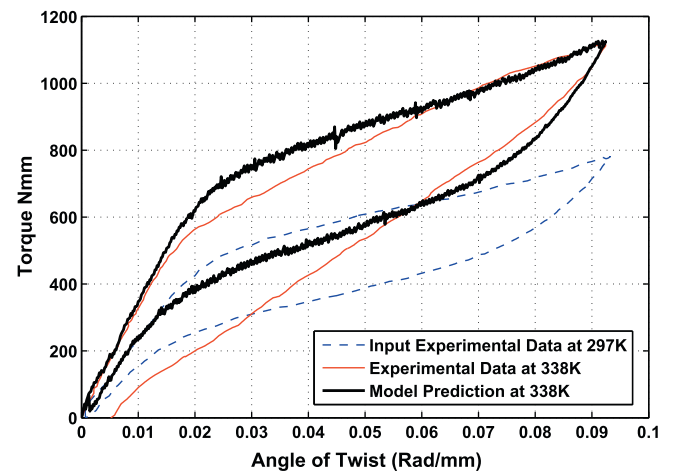
hysteresis exactly for a partially transformed case then one would have to recompute the hysterons for the each temperature case.

8.3.2. Simulation and model predictions for SMA wire response at different temperatures

Fig. 11(a) and (b) shows the model prediction at temperatures 297 and 338 K using the hysterons generated with the 297 K results as the data input. The experimental results at both temperatures were conducted at a frequency of 0.01 Hz obtained from Doaré et al. (2011). The greater extent of transformation in the case of wires is evident from the estimation of driving force – volume fraction plot as shown in Fig. 5(b) when compared against driving force – volume fraction estimation for springs as shown in Fig. 4(b). Parameters need not be recomputed for predicting response at different temperatures as the same hysterons generated in the 297 K case were used to estimate the response at 338 K. With higher temperature above A_f , the higher is the critical torque required for transformation and thus lesser is the transformation from austenite to SIM when compared against the same maximum deformation (450° twist). The model predictions at higher temperatures doesn't match exactly as the “extent of transformation” is different in each case due to the fact both the tests were unloaded after 450° twist (Doaré et al., 2011). Hence exact prediction of hysteresis could not be possible for such a case.



(a) Model prediction for 297K using the input data at 297K



(b) Model prediction for 338K using the input data at 297K

Fig. 11. Prediction for responses at temperatures 297 and 338 K using the hysterons generated at 297 K. The results for both temperatures were obtained from Doaré et al. (2011). The average error for this case was around 19%.

8.4. Simulation of SMA wire response for different diameter wires

The model was also used to predict the torsional response of two different wire diameters using the response for one diameter results as input. Chapman et al., 2011 in their recent work reported experimental data for NiTi wires under torsion for three different diameters (viz. 0.018", 0.02" and 0.023") under isothermal conditions at 296 K as shown in Fig. 3 of Chapman et al., 2011. Model prediction for diameters 0.018" and 0.023" using the model prediction at 0.02" results. Only the term " G_d " and " G_m " were changed depending on the diameter of wire chosen for prediction and the remaining model parameters were unchanged for predicting response. Fig. 12(a) and (b) shows the model predictions for 0.018" and 0.023" dia case using hysterons generated in the 0.02" dia and the results show a close match. It must be pointed out that in the experimental results reported by Chapman et al. for three different diameters the "unloading point" selected is different for each diameter case. They claim to have selected the "unloading points" as "limits of transformation region" for each diameter case by testing each wire diameter specimen until failure (Chapman et al., 2011). If one assumes complete transformation for each case, the elastic deformation of stress induced martensite (SIM) would

be different as the unloading points chosen are different for each diameter case (evident in Fig. 2 from their work Chapman et al., 2011). This would mean that the net hysteresis area when compared for the three diameters are different. So the use of same hysterons might not predict the hysteresis exactly unless "extent of transformation" in each case is the same.

Prediction of the results at different diameters is just an added feature of this model in addition to prediction of responses at different temperatures. It must be noted that predicting the torsional responses of different wire diameters using the response of one wire diameter is based on the assumption that the topology of the wire considered are the same. If a hollow and a solid wire with "equal polar moment of inertia" were loaded to the same torque, then the "extent of transformation" in the hollow wire would be greater compared to the solid wire as the untransformed austenitic core (due to really small shear strains) in hollow wire is no longer an issue at higher torque levels. Hence the prediction of responses for the same material at different diameters can be generalized if the topology of the specimen is the same and the specimens are subjected to the same "extent of transformation". Due to paucity of available experimental data on pure torsion for different wire diameters, only one case was verified.

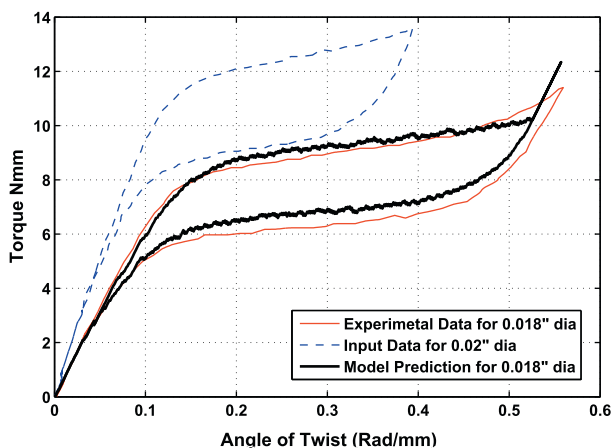
Torsional response of hollow SMA tubes/springs have also been of interest lately due the possibility that "hollow springs" could be a great way to harness SME/SE effects as they could be heated or cooled internally (see Baz et al. (1987), Keefe and Carman (2000), Hartl and Lagoudas (2007), Spinella and Dragoni (2010), Chapman et al. (2010), Takahashi (2010), Spaggiari et al. (2011) and Khan and Srinivasan (2011) for more discussions on hollow SMA springs/tubes and their applications).

8.5. Average error estimation: model prediction v/s experimental results

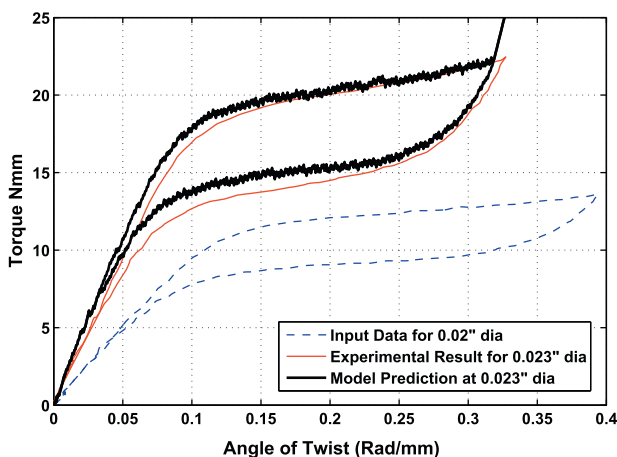
In a regular torsion test, the quantity "extent of transformation" is not experimentally measured and here this quantity is estimated using the torque-angle of twist data as shown in Section 4.3 i.e using driving force – martensitic volume fraction expressions (17) and (13). Given the test conditions and the fact that model predictions are based on hysterons generated from one experimental result as input data, an average error between the model predictions and the corresponding experimental results were estimated for each case. The average errors were estimated using the trapezoidal integration rule (trapz command in MATLAB®). The average error is an estimate for that specific case as the model predictions could be different depending on the hysterons calculated for predictions (i.e the choice of initial experimental data as input). The average error for each of model predictions discussed in this work are highlighted in Figs. 9(a), 10–12.

9. Conclusions

In this work, the significance of formulating a model by combining thermodynamics principles along with Preisach models to predict the superelastic torsional response of shape memory alloy (SMA) springs and wires is illustrated. The model is constructed based on experimentally measurable quantities torque and angle of twist, rather than solving for non-homogeneous shear stresses, strains directly across the wire cross-section. The key idea here was in separating the elastic and the dissipative part of the hysteretic response with a Gibbs potential based formulation and further employing Preisach models for modeling the hysteretic response. Such an approach can simultaneously include both thermal and mechanical loading in the same framework with the capability of simulating both load and displacement controlled experiments.



(a) Model prediction for 0.018" diameter using the input data for 0.02" diameter results



(b) Model prediction for 0.023" diameter using the input data for 0.02" diameter results

Fig. 12. Prediction for responses at different diameters 0.018" and 0.023" using the hysterons generated at 0.02". The experimental results for all cases were obtained from Chapman et al. (2011). Model results show a close match with the experimental results with an average error $\sim 7\%$ for both cases.

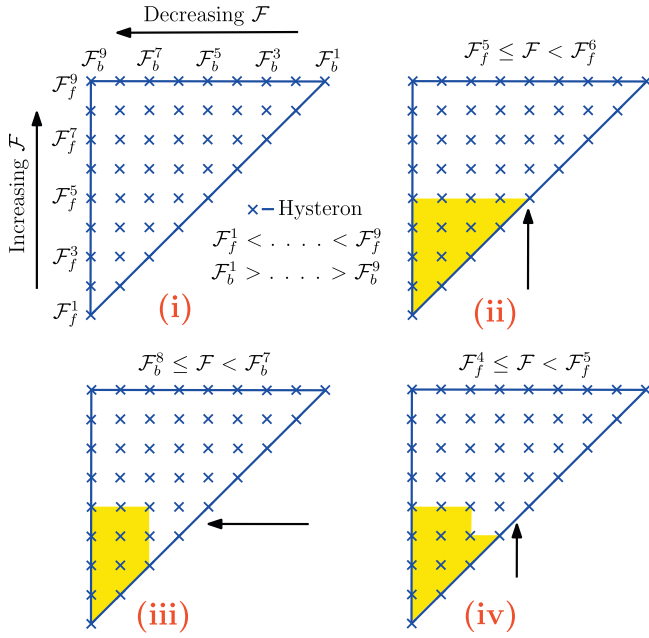


Fig. 13. Preisach Triangle – A systematic way for assigning switch on and switch off of the hysterons. The directions of loading (forward) and unloading (backward) sweeps are marked on the figure. Sub figures (ii), (iii), (iv) shows an example for sequencing of states in the Preisach triangle. The colored section shows the hysterons that are switched on with the corresponding driving force enforcing the state at the top of the state.

Further, it allows for easy handling of temperature variations observed in superelastic responses of SMA. The model results are compared with experimental results conducted on SMA springs and wires at different temperatures. The model was also used to predict torsion response of SMA wire at three different diameters using experimental data for one diameter. An average error between the model predictions and corresponding experimental results were estimated for each case (<10% for most cases). The error estimation is specific for each comparison case based on the test conditions and the experimental trial initially chosen for model predictions or generation of hysterons. The model was also used to predict response at different twists using the response at the highest twist. Prediction of torque v/s angle of twist response of SMA springs and wires could greatly facilitate designers in designing components experiencing torsional loading conditions for various engineering applications.

Acknowledgements

We acknowledge the support of the National Science Foundation CMMI Grant 1000790 in carrying out this work. We thank Dr. V. Buravalla from GE, India for useful discussions. We would like to thank Dr. T. Creasy from Texas A&M University for allowing us to use the Instron 5567 series machine to test SMA springs for experimental verification. We would also like to thank two anonymous reviewers for their suggestions.

Annex A. Preisach algorithm

The state S_i of the i 'th hysteron can take on one of two values: 0 or $\Delta\alpha^i$ where $\Delta\alpha^i$ is the volume fraction of martensite contributed by the i 'th hysteron. At any stage, the extent of transformation, i.e., the volume fraction of martensite evolved, is given by:

$$\alpha = \sum_{i=1}^n S_i \quad (\text{A.1})$$

The state $S_i^{(n)}$ at time t_n is known and hence the state at t_{n+1} is given by:

$$\text{if } S_i^{(n)} = 0 \ \& \ \mathcal{F}^{(n+1)} > \mathcal{F}_{\text{forward}}^i \quad (\text{A.2})$$

$$\text{then } S_i^{(n+1)} = \Delta\alpha_i \quad (\text{A.3})$$

$$\text{if } S_i^{(n)} = \Delta\alpha_i \ \& \ \mathcal{F}^{(n+1)} < \mathcal{F}_{\text{backward}}^i \quad (\text{A.4})$$

$$\text{then } S_i^{(n+1)} = 0 \quad (\text{A.5})$$

$$\text{else } S_i^{(n+1)} = S_i^{(n)} \quad (\text{A.6})$$

At the end of this time step, the $\alpha^{(n+1)}$ is then (as in A.1),

$$\alpha^{(n+1)} = \sum_{i=1}^n S_i^{(n+1)} \quad (\text{A.7})$$

Thus, at the end of the time step t_{n+1} , $\alpha^{(n+1)}$ is known, given $\mathcal{F}^{(n+1)}$ and $S_i^{(n)}$ for all the hysterons.

For each hysteron, inelastic power δP_{inel}^i is given by,

$$\delta P_{\text{inel}}^i = \mathcal{F} \delta\alpha \quad (\text{A.8})$$

$$= (\mathcal{F} - \mathcal{F}_{\text{mean}}) \delta\alpha + \mathcal{F}_{\text{mean}} \delta\alpha \quad (\text{A.9})$$

where $\delta\alpha$ is

$$\Delta\alpha_i \text{ if } \mathcal{F} > \mathcal{F}_{\text{forward}}^i \text{ or } \\ -\Delta\alpha_i \text{ if } \mathcal{F} < \mathcal{F}_{\text{backward}}^i$$

Therefore, the first term in Eq. (A.9) is always positive and the second term is positive or negative depending on $\delta\alpha$. The dissipation in a closed cycle of state (i.e. sum of δP_{inel}^i over all hysterons) will always be positive as the first term will be positive whereas the sum of second term will be zero. Using the above algorithm, the three parameters $\mathcal{F}_{\text{forward}}^i$, $\mathcal{F}_{\text{backward}}^i$ and $\Delta\alpha^i$ are computed for each hysteron and the driving forces ($\mathcal{F}_{\text{forward}}^i$, $\mathcal{F}_{\text{backward}}^i$) assigned in a systematic way as described in Fig. 13. This greatly simplifies the computation of $\Delta\alpha^i$ for each of the hysterons.

References

- Aguilar, R., Savi, M., Pacheco, P., 2010. Experimental and numerical investigations of shape memory alloy helical springs. *Smart Materials and Structures* 19, 025008.
- Baz, A., Iman, K., McCoy, J., 1987. Active control of flexible space structures using the nitinol shape memory actuators. Technical Report. DTIC Document.
- Bellini, A., Colli, M., Dragoni, E., 2009. Mechatronic design of a shape memory alloy actuator for automotive tumble flaps: a case study. *IEEE Transactions on Industrial Electronics* 56, 2644–2656.
- Bo, Z., Lagoudas, D., 1999. Thermomechanical modeling of polycrystalline smas under cyclic loading, part IV: Modeling of minor hysteresis loops. *International Journal of Engineering Science* 37, 1205–1249.
- Bo, Z., Lagoudas, D.C., Miller, D., 1999. Material characterization of sma actuators under nonproportional thermomechanical loading. *Journal of Engineering Materials and Technology* 121, 75–85.
- Boyd, J., Lagoudas, D., 1996. A thermodynamical constitutive model for shape memory materials. part I. The monolithic shape memory alloy. *International Journal of Plasticity* 12, 805–842.
- Callen, H., 1985. *Thermodynamics and an Introduction to Thermostatistics*. Wiley-VCH, ISBN 0-471-86256-8, Herbert B. Callen (ed.), pp. 512.
- Chapman, C., Eshghinejad, A., Elahinia, M., 2011. Torsional behavior of niti wires and tubes: Modeling and experimentation. *Journal of Intelligent Material Systems and Structures* 22, 1239–1248.
- Chapman, C., Karbaschi, Z., Elahinia, M., Tabesh, M., 2010. Torsional behavior of shape memory alloy tubes for biomedical applications. *ASME*.
- Doaré, O., Sbarra, A., Touzé, C., Moussa, M., Moumni, Z., 2011. Experimental analysis of the quasi-static and dynamic torsional behaviour of shape memory alloys. *International Journal of Solids and Structures*.
- Doraiswamy, S., Rao, A., Srinivasa, A., 2011. Combining thermodynamic principles with preisach models for superelastic shape memory alloy wires. *Smart Materials and Structures* 20, 085032.
- Ghosh, P., Rao, A., Srinivasa, A.R., 2013. Design of multi-state and smart-bias components using shape memory alloy and shape memory polymer composites. *Materials and Design* 44, 164–171.
- Ghosh, P., Srinivasa, A., 2011. A two-network thermomechanical model of a shape memory polymer. *International Journal of Engineering Science*.

- Hartl, D., Lagoudas, D., 2007. Aerospace applications of shape memory alloys. *Proceedings of the Institution of Mechanical Engineers, Part G: Journal of Aerospace Engineering* 221, 535.
- Keefe, A., Carman, G., 2000. Thermo-mechanical characterization of shape memory alloy torque tube actuators. *Smart Materials and Structures* 9, 665.
- Khan, E., Srinivasan, S., 2011. A new approach to the design of helical shape memory alloy spring actuators. *Smart Materials Research*.
- Khandelwal, A., Buravalla, V., 2011. Models for shape memory alloy behavior: an overview of modeling approaches. *The International Journal of Structural Changes in Solids* 1, 111–148.
- Ktena, A., Fotiadis, D., Spanos, P., Massalas, C., 2001. A preisach model identification procedure and simulation of hysteresis in ferromagnets and shape-memory alloys. *Physica B: Condensed Matter* 306, 84–90.
- Lagoudas, D., 2008. *Shape Memory Alloys: Modeling and Engineering Applications*. Springer Verlag.
- Liang, C., Rogers, C., 1990. One-dimensional thermomechanical constitutive relations for shape memory materials. *Journal of Intelligent Material Systems and Structures* 1, 207–234.
- Maganzini, A., Wong, A., Ahmed, M., 2010. Forces of various nickel titanium closed coil springs. *The Angle Orthodontist* 80, 182–187.
- Manhartsberger, C., Seidenbusch, W., 1996. Force delivery of ni-ti coil springs. *American Journal of Orthodontics and Dentofacial Orthopedics* 109, 8–21.
- Mayergoyz, I., 1986. Mathematical models of hysteresis. *IEEE Transactions on Magnetics* 22, 603–608.
- Mayergoyz, I., Service, S.O., 2003. *Mathematical Models of Hysteresis and Their Applications*. Elsevier.
- MirzaeiFar, R., DesRoches, R., Yavari, A., 2010a. A combined analytical, numerical, and experimental study of shape-memory-alloy helical springs. *International Journal of Solids and Structures*.
- MirzaeiFar, R., DesRoches, R., Yavari, A., 2010b. Exact solutions for pure torsion of shape memory alloy circular bars. *Mechanics of Materials* 42, 797–806.
- Miura, F., Mogi, M., Ohura, Y., Karibe, M., 1988. The super-elastic Japanese niti alloy wire for use in orthodontics part iii. studies on the Japanese niti alloy coil springs. *American Journal of Orthodontics and Dentofacial Orthopedics* 94, 89–96.
- Miyazaki, S., Otsuka, K., 1989. Development of shape memory alloys. *ISIJ International* 29, 353–377.
- Müller, I., Seelecke, S., 2001. Thermodynamic aspects of shape memory alloys. *Mathematical and Computer Modelling* 34, 1307–1355.
- NDC, Nitinol. Website. <<http://www.nitinol.com>>
- Ortín, J., 1992. Preisach modeling of hysteresis for a pseudoelastic cu–zn–al single crystal. *Journal of Applied Physics* 71, 1454–1461.
- Otsuka, K., Ren, X., 2005. Physical metallurgy of ti–ni-based shape memory alloys. *Progress in Materials Science* 50, 511–678.
- Paiva, A., Savi, M., Braga, A., Pacheco, P., 2005. A constitutive model for shape memory alloys considering tensile-compressive asymmetry and plasticity. *International Journal of Solids and Structures* 42, 3439–3457.
- Qidwai, M., Lagoudas, D., 2000. Numerical implementation of a shape memory alloy thermomechanical constitutive model using return mapping algorithms. *International Journal of Numerical Methods Engineering* 47, 1123–1168.
- Rajagopal, K.R., Srinivasa, A.R., 1999. On the thermomechanics of shape memory wires. *Zeitschrift für Angewandte Mathematik und Physik (ZAMP)* 50, 459–496.
- Savi, M., Paiva, A., 2005. Describing internal subloops due to incomplete phase transformations in shape memory alloys. *Archive of Applied Mechanics* 74, 637–647.
- Schneevoigt, R., Haase, A., Eckardt, V., Harzer, W., Bourauel, C., 1999. Laboratory analysis of superelastic niti compression springs. *Medical Engineering and Physics* 21, 119–125.
- Shaw, J., 2000. Simulations of localized thermo-mechanical behavior in a niti shape memory alloy. *International Journal of Plasticity* 16, 541–562.
- Shaw, J., Kyriakides, S., 1995. Thermomechanical aspects of niti. *Journal of the Mechanics and Physics of Solids* 43, 1243–1281.
- Spaggiari, A., Spinella, I., Dragoni, E., 2011. Design of a telescopic linear actuator based on hollow shape memory springs. *Journal of Materials Engineering and Performance* 20, 489–496.
- Speicher, M., Hodgson, D., DesRoches, R., Leon, R., 2009. Shape memory alloy tension/compression device for seismic retrofit of buildings. *Journal of Materials Engineering and Performance* 18, 746–753.
- Spinella, I., Dragoni, E., 2010. Analysis and design of hollow helical springs for shape memory actuators. *Journal of Intelligent Material Systems and Structures* 21, 185–199.
- Spinella, I., Dragoni, E., Stortiero, F., 2010. Modeling, prototyping, and testing of helical shape memory compression springs with hollow cross section. *Journal of Mechanical Design* 132, 061008.
- Spinella, I., Scirè Mammano, G., Dragoni, E., 2009. Conceptual design and simulation of a compact shape memory actuator for rotary motion. *Journal of Materials Engineering and Performance* 18, 638–648.
- Stoeckel, D., 1990. Shape memory actuators for automotive applications. *Materials and Design* 11, 302–307.
- Takahashi, M., 2010. Shape Memory Alloy Actuator. US Patent 7 (788), 921.
- Tanaka, K., 1986. A thermomechanical sketch of shape memory effect: one-dimensional tensile behavior. *Research Mechanics* 18, 251–263.
- Tobushi, H., Tanaka, K., 1991. Deformation of a shape memory alloy helical spring (analysis based on stress–strain–temperature relation). *JSME International Journal. Series 1 Solid Mechanics, Strength of Materials* 34, 83–89.
- Tripolt, H., Burstone, C., Bantleon, P., Manschiebel, W., 1999. Force characteristics of nickel–titanium tension coil springs. *American Journal of Orthodontics and Dentofacial Orthopedics* 115, 498–507.
- Von Fraunhofer, J., Bonds, P., Johnson, B., 1993. Force generation by orthodontic coil springs. *The Angle Orthodontist* 63, 145.
- Wayman, C., 1992. Shape memory and related phenomena. *Progress in Materials Science (UK)* 36, 203–224.